HiSST: 2nd International Conference on
High-Speed Vehicle Science & Technology
11–15 September 2022, Bruges, Belgium

# An overview on the use of CFD in the development of hypersonic vehicles at Destinus.

*Jimmy-John O.E. Hoste*[1], *Dominique Charbonnier*[2], *Andrés Zarabozo*[3],
Ambara Bernabeu-Vazquez[4], Tomasz Witkowski[5]

## Abstract

This paper presents an overview of the use of CFD to help in the design of various aspects of the Destinus hyperplanes. CFD is not only relied upon in the aerodynamic shape definition but also in engine related design tasks including intakes, compressors, turbines, nozzles as well as feeding components. The different tasks are complementary to rapid engineering design tools and aim at improving general in-house understanding, semi-empirical modeling capability as well as build surrogate models. Furthermore, the affordability of CFD can be taken advantage of at much earlier stages in design and development tasks. The versatility of such an endeavour requires a robust CFD solver capable of tackling a diverse range of conditions, from subsonic to hypersonic, with associated physics such as chemical reactions for ideal and real gases, multi-phase flows and conjugate heat transfer. To this end, the commercial software Simcenter STAR-CCM+ is intensively used at Destinus.

**Keywords:** *CFD, hypersonics, propulsion, mixing, combustion*

## 1. Introduction

Computational Fluid Dynamics (CFD) has gained an important place in general vehicle design which has been boosted by a more widespread availability of computational power with relative affordability. This development has made CFD the ad-hoc tool to complement wind tunnel and flight testing as demonstrated by the literature in the past two decades with hypersonic flight test programs such as the X43 [1], X51 [2], HyShot [3], HIFiRE [4], IXV [5, 6] and the more recent BOLT program [7, 8]. The growing role of CFD in aerospace design, understood by academia, research centres and industry, has led to the compilation of the CFD Vision 2030 Roadmap, contracted by NASA [9]. The roadmap's intend was to identify current (as of 2014) shortcomings and bottlenecks of CFD and provide strategic key points to guide the path forward. This also includes CFD related topics such as meshing, multi-disciplinary design optimization (MDO) as well as the rapidly evolving hardware architecture of computers and High Performance Computing (HPC). From a physics point of view, accurate turbulence modeling has been identified as a large shortcoming of CFD, a topic which is as well very actual in hypersonic environments and has motivated some of the HiFIRE tests as well as the BOLT program. Possible steps include moving to scale-resolving simulations such as Hybrid RANS/LES, DES or LES. Combustion CFD is another topic of interest which has to mature. A midway point evaluation of the roadmap has been published in 2020 with details on steps taken in tackling the different challenges and increase the maturity [10]. The roadmap plays an important role in the advent of Simulation Based Certification which aims at increasing the digital role in aerospace related certification processes and could therefore reduce the time to do so.

While it is true that improved predictive capability of CFD can be achieved through scale-resolving simulations, the large computational requirements of such techniques make it impractical for design

[1] *Destinus SA, Aerothermodynamics Engineer, jimmyjohn.hoste@destinus.com*
[2] *Destinus SA, Lead Aerothermodynamics Engineer*
[3] *Destinus SA, Aerothermodynamics Engineer*
[4] *Destinus SA, Propulsion Engineer*
[5] *Destinus Germany GmbH, Turbomachinery Engineer*

purposes (at least in early design phases). The same computational requirements remain a limiting factor for general combustion simulations. Nonetheless, the ever-growing computational resources have enabled more routine use of CFD for early design purposes. It is important to note that CFD does not (yet) replace what can be considered low-fidelity tools, especially in conceptual design phases where massive amount of evaluations need to be performed in short times.

Destinus is in the process to develop hydrogen-powered hypersonic vehicles - hyperplanes, and in doing so makes the most of CFD to help in various designs where possible. These designs involve all aspects of hypersonic vehicles ranging from the external aeroshape and aerothermal characterization to internal flow paths related to the engine integration as well as the engine design and associated components. The need to be able to rely on CFD for a variety of fluid (and solid) flow problems leads to the careful selection of a CFD framework to do so. Whilst there are many open-source solvers out there, finding a single framework to handle the various problems would be difficult. We would need to handle subsonic to hypersonic flows with associated thermochemistry, real gas flows, multi-phase flows, conjugate heat transfer and advanced combustion modeling. Using multiple CFD solvers could be an option with increased probability of different input and output formats. External meshers would also have to be used for more complex geometries. Lastly, dependent on the CFD solver, extensive validation exercises would have to be performed which requires dedicated human resources that cannot be mobilized for actual design work. Given these different constraints, the use of commercial CFD software becomes more attractive. At Destinus, we partnered up with Simcenter STAR-CCM+[11] to tackle the challenges ahead. Being at the forefront of aerospace design, it is not unexpected that certain applications will push the boundaries of current state-of-the-art of commercial CFD softwares. This is especially true in many challenges related to hydrogen technology or hypersonic flow conditions.

This paper will give an insight in the type of problems tackled with CFD to help make diverse design decisions. A first section (Section 2) will succinctly introduce the CFD solver. The following section (Section 3) will be dedicated to external flow related problems while another one to internal flows (Section 4). Finally an outlook on future type of problems will be given followed by conclusions.

## 2. CFD solver

The CFD related work at Destinus is performed with Simcenter STAR-CCM+ [11]. This multi-physics environment provides a collection of solvers to handle various problems. Similarly to other commercial softwares, a vast number of validation and verification test cases were tackled by the developers and application engineers. Relevant to external hypersonic flow fields, an extensive sensitivity study has been performed by Cross and West [12] on standard hypersonic double cone, cylinder-flares and sphere-like geometries widely used in the literature. In addition, relevant to hypersonic internal flow paths, a stand-alone shock-boundary layer interaction setup [13] and the SCHOLAR scramjet experiment [14] were used by Siemens for validation purposes.

A powerful feature of Simcenter STAR-CCM+ is the swift and robust meshing capability and has been much appreciated by the engineers at Destinus. The majority of the test cases has been simulated with polyhedral meshes with some exceptions where quadrilateral or hexagonal grids have been preferred. In terms of settings, most of the default solver settings are kept with some case specific changes required such as the inviscid flux treatment in supersonic / hypersonic conditions. For reacting cases, the Chemkin format is used to specify species and reactions.

The Java API feature is also heavily used in aerodynamic database generations and other parametric sweeps as it allows to easily loop through simulations varying diverse settings. Moreover, it has demonstrated to be very practical for monitoring and post-processing purposes. The following sections will detail the use of STAR-CCM+ with some examples from Destinus test cases.

## 3. External flows

The development of an hyperplane does require the ability to fly in subsonic, supersonic and hypersonic regimes. Each regime has it's own challenges linked to the attitude of the hyperplane and must be

tackled in the external shape design. Subsonic flight will, for instance, be characterized by higher angle of attacks (AoAs) (take-off, landing) while supersonic and hypersonic flight will occur at lower angles of attack. From a CFD point of view, each of these regimes comes with its own modeling challenges. Lower speeds and higher AoAs needs turbulence modeling capability to predict separation behavior. As pointed out in the CFD vision 2030 [9, 10], turbulence modeling's predictive capability is a subject that must be considerably advanced. This statement is also valid for hypersonic flows [15]. Supersonic speeds require shock capturing and hypersonic speeds, in addition to shock capturing, accounting for high heat loads and possibly thermo-chemical non-equilibrium effects. The latter effect depend strongly on the speed and flight altitude as discussed by Longo *et al.* [16].

CFD has clearly a role to play in external aeroshape design, especially at hypersonic speeds where flight test is not yet accessible and experimental ground test facilities are scarce and costly to operate. Moreover, hypersonic wind tunnels typically does not allow full scale testing. The realization that CFD can heavily be relied upon in design of hyperplanes is exemplified by Cockrell [17], and with the increased (cheap) availability of computational resources, has been widely adopted in various national and international programs in the past two decades as discussed in Section 1.

The following Subsections will discuss the use of CFD in external aeroshape related design activities at Destinus. It includes the preliminary analyses of the hyperplane's outer mold line (OML), aerothermal aspects of vehicles, and intake integration. Moreover, as Destinus has a flying test lab, a correlation activity between flight test and CFD will be detailed.

### 3.1. Aeroshape design

A very involved activity in hyperplane design its the definition of the vehicle's shape (OML) itself. In design space exploration, CFD can start to play a role by providing the aerodynamic coefficients required for mission analysis as well as the loads for structural design. The modeling assumption to do so is considering the flow to be inviscid (Euler CFD computations). Viscous simulations, undoubtedly required for detailed design, are already too costly in this early design phases. Nevertheless, a few sanity check points in the flight envelope of interest should be performed, especially in subsonic, high AoAs attitudes.

The first generations of aerodynamic databases (AEDB) for the different concepts investigated at Destinus were made, as mentioned above, applying inviscid Euler computations plus friction drag correlations by mean of engineering formula, in order to take into account additional viscous effects. This methodology is generally used in the conceptual and preliminary design phases, when one wishes to use CFD for a reasonable computational cost, to study a large number of configurations, or variations of parameters. For hypersonic vehicles, one can mention non-exhaustively the STRATOFLY, HIFiRE4, SpaceShipTwo projects [18],[4],[19], where this methodology was applied.

As a starting point, the engineering formula proposed in [18] was used at Destinus in combination with inviscid Euler computations performed with STAR-CCM+. The drag coefficient can be expressed as:

$$C_D = C_{Dinviscid} + \Delta C_{Dviscous} \tag{1}$$

where $C_{Dinviscid}$ comes from the CFD inviscid Euler simulation and $\Delta C_{Dviscous}$ is the viscous contribution coming from the engineering formula. This contribution can be written as:

$$\Delta C_{Dviscous} = \alpha * \frac{1}{[Log(Re)]^{2.58}} * \frac{1}{(1+\beta * M^2)^{\gamma}} * \frac{A_{wetted}}{A_{ref}} \tag{2}$$

where $Re$ is the Reynolds number, $M$ the Mach number and $A_{wetted}$ / $A_{ref}$ the wetted area of the vehicle and the reference surface, respectively. The three parameters $\alpha$, $\beta$ and $\gamma$ are dependant on the vehicle configuration considered. These coefficients have to be tuned by means of viscous CFD simulations for a set of Mach numbers representative of the mission. As a first guess, the parameters reported in [18] where selected by default, since initially, the concepts considered at Destinus are of the same class of vehicles. These coefficients are set to $\alpha = 0.43$, $\beta = 0.31$ and $\gamma = 0.37$.

An evaluation of this method is presented below, for a generic hypersonic vehicle concept. The concept considered is composed of a fuselage designed as a cylinder truncated at the bottom with ogive shaped nose and tail, a delta wing and a single vertical tail plane. CFD simulations with STAR-CCM+ have been performed on this model: ten with inviscid Euler assumption, and five as Reynolds-Averaged Navier-Stokes (RANS) simulation using Spalart-Allmaras [20] turbulence modeling, covering the flight regimes from subsonic (M=0.3) to low hypersonic (M=6). Two different polyhedral meshes were generated on an half configuration, with around 1M cells for Euler simulations, and around 4M cells for RANS simulations including prismatic layers at the wall with suitable parameters for turbulence modeling.

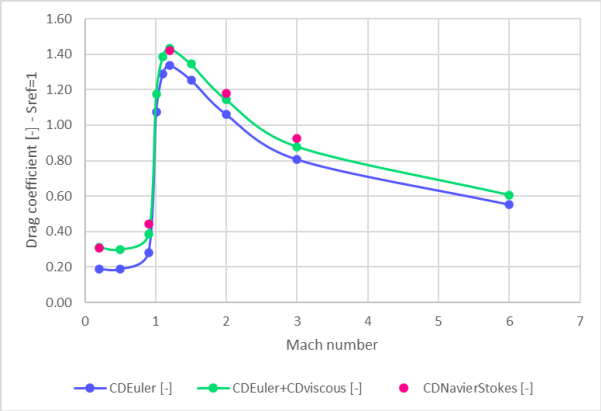


**Fig 1.** Comparison of Drag coefficient for Euler, Euler + viscous correlations and RANS simulations, at AoA=0

The results concerning the estimation of the drag are represented in Figure 1. The drag coefficient (for a reference surface of 1) is reported for the different flight conditions, at zero angle of attack. The blue curve shows the results of the inviscid Euler computations, the green curve shows the results of the inviscid Euler simulation to which the viscous correlations $\Delta C_{D_{viscous}}$ given by the formula detailed above are applied, and the pink points highlight the viscous Navier-Stokes results. One can observe that for this configuration, and these flight conditions, the inviscid Euler simulations with viscous correlations (green) are in very good agreement with the results of the Navier-Stokes simulations (pink). The generation of an AEDB, useful for mission analysis, by applying this methodology allows for a substantial reduction in computational time, while keeping an estimation of the key aerodynamic quantities close to those obtained by much more expensive Navier-Stokes simulations. At preliminary design stage of Destinus hypersonic vehicles, it appears as a good balancing between accuracy and computational effort.

In addition, for AEDB generation, automation and simulation time are key. STAR-CCM+ Java API (see section 2) proved very valuable for quickly setting up simulation loops with all the automated post-processing. Using macros, it is possible to automate the entire process from importing a CAD to exporting results. STAR-CCM+ integrated CAD tool and automatic mesher are very robust, which can simplify the preprocessing to simply launching a macro. Not so long ago preprocessing and meshing was a very manual task that could take weeks or even months. Of course, specific tuning must be taken care depending on the model or application. As mentioned previously, simulation time is also very important when running large loops. With 48 core workstations, it is possible to run an 1M cells inviscid simulation in about 5 minutes. This means that in 60 hours (one weekend) it is possible to run around 700 simulations. Naturally, higher fidelity models, including viscosity and localized mesh refining, still requires longer computational times and / or an increase in computational power.

### 3.2. Aerothermal design

Hypersonic heat transfer is an important field of work in Destinus' future hyperplanes. Current prototypes are still much slower and don't need to worry about skin thermal problems. Nonetheless, some analyses

are being performed in preparation for the future. Some dedicated teams are already looking into, for instance, active cooling solutions as well as effect of heat transfer on the structure. An example of an analysis performed is the effect of non-smooth surfaces on the heat transfer as depicted in Figure 2. The simulation shown uses Menter's SST [21] turbulence model with isothermal walls on an ≈1M cells. Generally, the strategy of extracting heat flux information from such a model in combination with an adiabatic simulation to extract surface temperature is adopted, as commonly found in hypersonic related literature. Different surface smoothness were simulated to study the effect of bumps on the key thermal parameters like wall temperature or wall heat flux. It was confirmed that this type of simulation is very sensitive to the surface mesh used. Various mesh types were analyzed with some differences between quad mesh and polyhedral mesh.

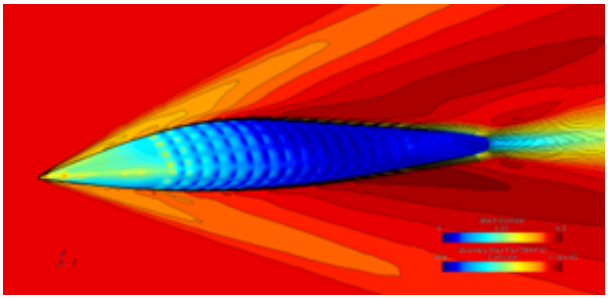

**Fig 2.** . Example of heat transfer study for non-smooth surfaces.

### 3.3. Stability and Control: correlating flight data with CFD

External aerodynamic computations are used to analyze the stability and control of OMLs. This subject is more challenging when studying airplanes that need to fly in subsonic, supersonic, and hypersonic regimes. For example, the centre of pressure changes from subsonic to supersonic, which affects the balancing and stability.

Hypersonic design are usually seen with tailless delta wings. Having no horizontal stabilizer makes stability and control a more complex task. Hypersonic shapes like HEXAFLY-INT [22] for example tend to pitch down when the CoG is located at a static longitudinal stable position. Using elevons for trimming at high speeds might not be viable for very high dynamic pressures, as the actuator might not be able to hold the hinge moment.

At Destinus, a first prototype named Jungfrau has been used to study hypersonic shapes flying at low speeds, and to validate simulations and devise methodologies. Jungfrau is a 4m radio-controlled aircraft with a shape inspired by the HEXAFLY-INT family [22] as seen in Figure 3. Initial flight test campaigns have been focusing on studying the subsonic stability and control of the aircraft and the performance of control surface like hinge moments. Figure 3 shows an example of flight test and CFD comparison. In this case, the objective is to study the aircraft performance during take-off. Rotation speeds and elevon performance is correlated with ground rolling tests. The aircraft accelerates on the runway with different elevon deflections until the rotation speed $v_r = \sqrt{\frac{W(x_{mlg}-x_{cg})}{0.5 c_{m,mlg} \rho}}$ is achieved ($W$ represents the vehicle's weight and subscript $cg$ refers to the center of gravity). CFD analyses with ground effect and elevon deflections are then correlated evaluating the pitch moment necessary to rotate around the main landing gear (mlg).

Figure 4 shows Jungfrau during a flight test with its associated CFD model. Initial work focused on longitudinal analyses. Lateral handling qualities and stability was subjectively evaluated by the pilot. Jungfrau was balanced to be at a stable position but with very low static margin. The low static margin is caused by its tendency to pitch down which requires elevons to trim the aircraft. The static margin and elevon trim position were also correctly predicted with CFD .

Figure 5 shows correlation results for hinge moments. Each point represents a single flight test point. Different data are collected during the test in order to estimate the hinge moment produced by the

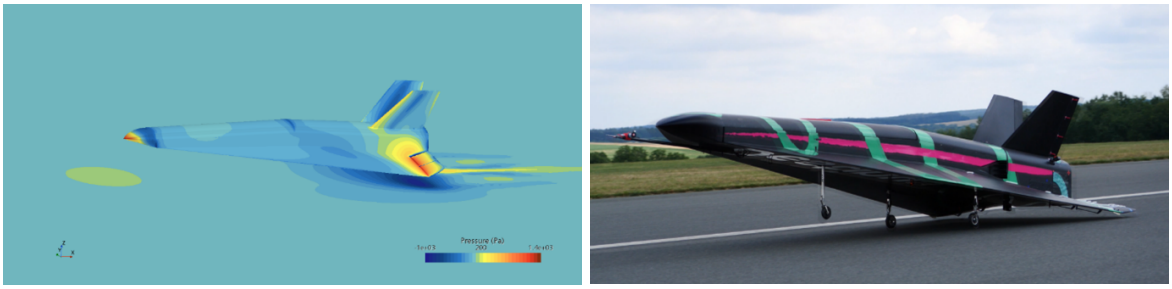

(a) (b)

**Fig 3.** Rotation speed correlation between (a) ground effect CFD simulations and (b) ground roll tests.

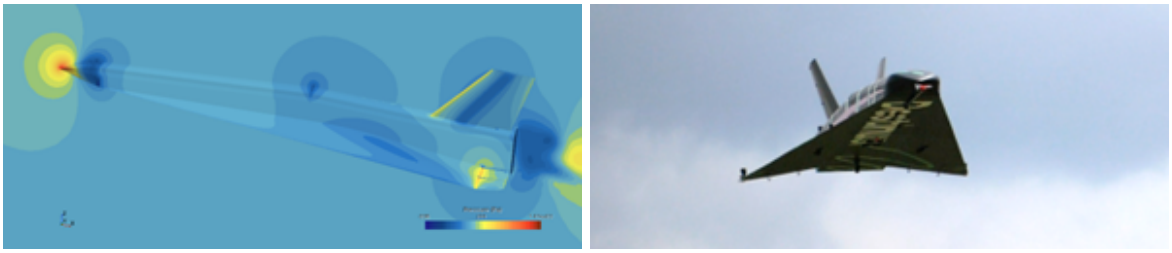

(a) (b)

**Fig 4.** Elevon and servos performance correlation between flight test and CFD

servo (taken from the servo power) and the flight conditions needed to predict the aerodynamic hinge moment (speed, atmospheric conditions, …). The line represents the ideal correlation where points are the same between CFD and Servo hinge moment. Results showed a very good correlation of the CFD prediction, both in magnitude and in the prediction of servo saturation.

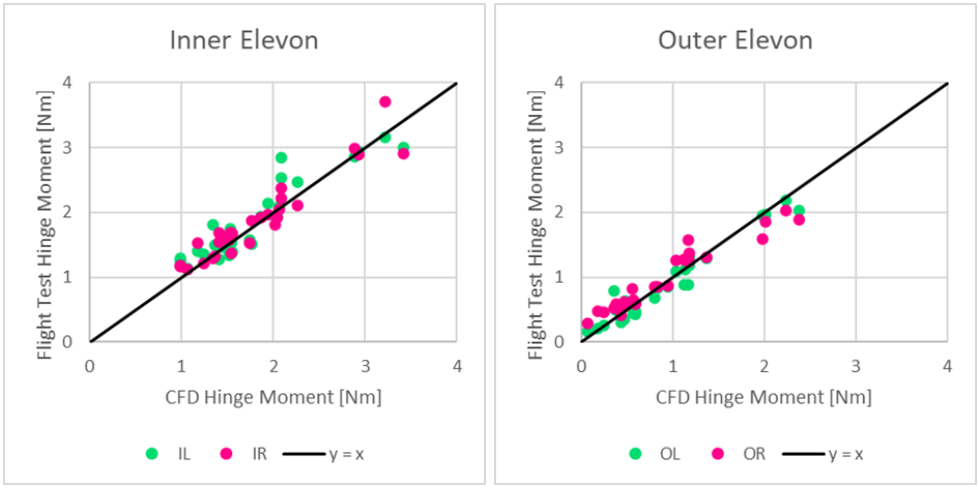


(a) (b)

**Fig 5.** Hinge Moment correlation results between CFD and Flight test

The methodology and tools developed are now used to help in the design and sizing of control surfaces for future prototypes. Understanding the load on the servos is important for preparing our second

prototype Eiger. For these exercises, CFD simulations were done using Euler models with meshes around 1 million cells. Some RANS, using Menter's SST model [21] and denser meshes (around 5 million cells) were performed for rapid validation.

### 3.4. Intake integration

Turbojet engines operating at supersonic speeds require an inlet that is able to reduce the mach number to its operating speeds. For fast intake design, a 1D model has been developed. CFD has been used as a validation and correlation tool. CFD validation has been done in various steps. First axisymmetric models were used to compare the Mach field and boundary layer predictions of the 1D model (as seen in Figure 6). The image show the initial correlations between 2D axi-symmetric CFD simulations, and the 1D model with boundary layer estimation. Axisymmetric CFD simulations can be easily run even on a laptop as they only contained about 100k elements. This first step allows to size the intake in order to generate, very rapidly, more complex 3D geometries specific for our vehicle's need. For example, one of the simplest inlets are pitot intakes which usually have rectangular entry that must transition into circular output into the engine's compressor. Pitot intakes is a viable option for Destinus prototypes that will fly at low subsonic speeds.

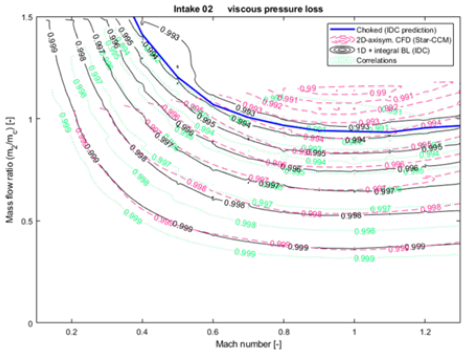


**Fig 6.** Correlation results between CFD and 1D model.

As aforementioned, 3D geometries are created using the 1D model and simulated with CFD. At this point only the internal flowpaths were simulated as models got heavier when having special care of the boundary layer evolution (Figure 7 (a)). Models remain small enough (2.5 million cells) to be able to simulate a wide range of points in the flight envelope. Finally, the intakes have also been simulated including interactions of the aircraft and external flow (Figure 7 (b)). This allows to study external phenomena like spillage drag or interactions between the fuselage boundary layer and the flow entering the intake. Including external effect doubled the number of cells needed to around 5 million. All the simulations in these studies were performed using Menter's SST model [21].

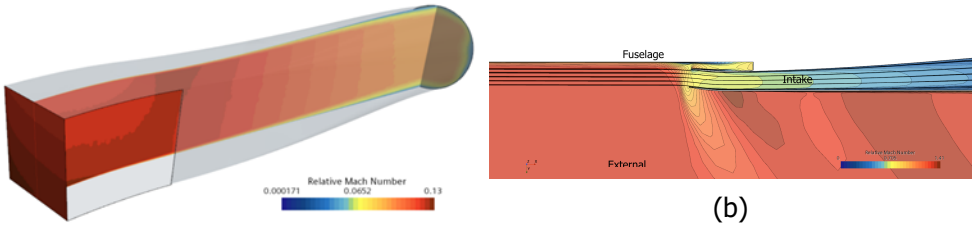


(a) (b)

**Fig 7.** Internal flow simulation of pitot intake (a) and Simulations of intake considering fuselage and external flow interaction (b)

## 4. Internal flows

Part of the work at Destinus is focused on propulsion design to enable hypersonic flight. This includes the development of an air-turbo-rocket (ATR) [23] for a segment of the flight envelope. A schematic of such an engine type is depicted in Figure 8 with associated components. CFD can be used to help in the design of these various components as will be discussed in the following subsections. Additional details on ATR-related design activities at Destinus can be found in [23].

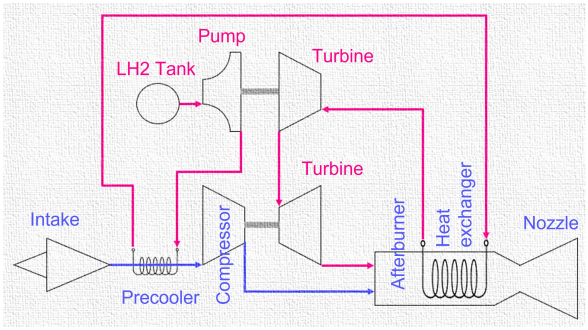


**Fig 8.** ATR schematic [23]

### 4.1. Compressor and Turbine

In the early design phase of the ATR engine, some design and optimization tasks have been subcontracted by Destinus to an external engineering company experienced in small gas turbine design, ReynoldsAero (RA). They performed a large number of CFD simulations to evaluate the performance of the compressor and the turbine parts of the ATR engine, for different operating ranges, and varying some design parameters. The simulations were performed using a popular CFD software in the field of turbomachinery, namely FINE™/TURBO from Cadence (originally NUMECA)[24]. At Destinus, the aim was to rebuild partially the CFD work done by RA, firstly to confirm the performance trends obtained by RA, and secondly to evaluate the capabilities of Simcenter STAR-CCM+ on such kind of turbomachinery simulations.

#### *4.1.1. Compressor*

The compressor stage consists of a rotor row including main blades and splitter blades, followed by two stator rows. Some initial simulations have been performed in STAR-CCM+ with the hexahedral mesh generated by RA using Cadence software, however the interface between the two stator rows highlighted an issue with the solver. Indeed, the computational domain in the hexahedral mesh was not coincident between the outlet of stator 1 and the inlet of stator 2, and STAR-CCM+ does not have periodicity boundary conditions compatible with this type of interface. Only a mixing plane condition is available, but in this case, between two stators, this condition is not optimal since it dissipates any wake propagation in the downstream wheel. Therefore, a computational domain was designed using Siemens NX CAD software, based on the original blade geometries, but including a continuous domain between the stator 1 and the stator 2 rows. Once the computational domain was defined, a polyhedral mesh was generated for one blade-to-blade passage, with periodic boundary conditions, as for the configurations computed by RA.

A fine mesh comprising 6M cells, and a coarse mesh comprising 0.9M cells have been generated, including prismatic layers at the wall with different clustering parameters. The target wall $y+$ value for turbulence modelling was fixed below 5 for the fine mesh without use of wall functions, while it was fixed above 30 on the coarse mesh with the use of "All $y+$ wall treatment" feature of the solver. Ideal gas was chosen as a fluid model and the two equation $k-\epsilon$ turbulence model [25] has been selected to match with the model used by RA. Standard sea level boundary conditions are applied for the inlet and at the outlet boundary the radial equilibrium condition is applied with fixed static pressure at the hub. Adiabatic and non-slip conditions are imposed at all the solid boundaries. Non-reflecting mixing plane approach is used for the rotor-stator interface. This approach allows to obtain steady solution at each row by performing an azimuthal average of the flow parameters at the interface to ensure the massflow and impulse conservation.

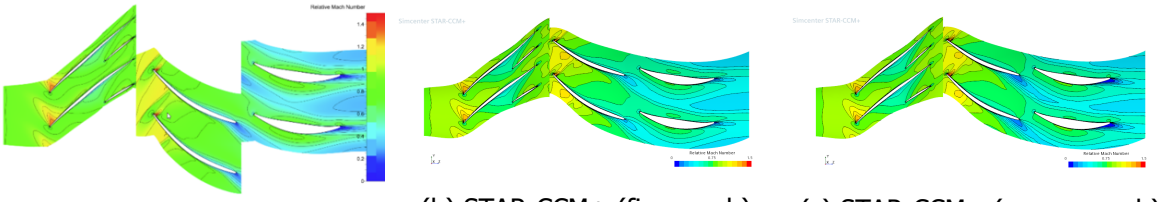

(a) FINE™/TURBO (b) STAR-CCM+ (fine mesh) (c) STAR-CCM+ (coarse mesh)

**Fig 9.** Relative Mach number distribution at 50% of blade span

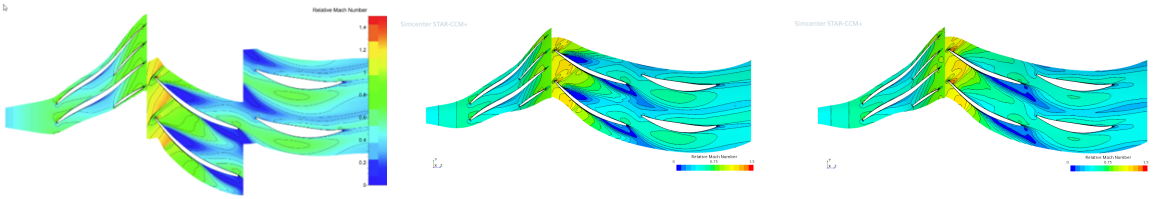

(a) FINE™/TURBO (b) STAR-CCM+ (fine mesh) (c) STAR-CCM+ (coarse mesh)

**Fig 10.** Relative Mach number distribution at 10% of blade span

The results of one selected simulation for the nominal rotating velocity are depicted in Figures 9 and 10 showing the relative Mach number distribution at two different percentages of blade span, respectively 50% and 10%, for two blade-to-blade passages. The computations performed with FINE™/TURBO (RA results) and with STAR-CCM+ (fine and coarse meshes) are reported with as much as possible a similar colormap in order to allow for a comparison of velocity levels. Globally, one can observe that the results are close with both solvers, as well as in between the fine and coarse meshes for STAR-CCM+ computations. On Figure 10 at 10% of blade span, the recirculation area occurring in the first stator row on the pressure side of the blade close to the leading edge, as well as on the suction side close to the trailing edge, is reported by both solvers. In contrast, the shock observed upstream the first stator blade in the FINE™/TURBO computation, Figure 10(a), is not clearly depicted in the STAR-CCM+ results, even with the fine mesh. This could be due to the fact that the interface between the rotor and the stator is not located at the same axial position, and the mixing-plane condition is applied a little further upstream in the case computed by RA. Nevertheless, looking at the global performance of the compressor, these discrepancies in the 3D flow field prediction have no major effects.

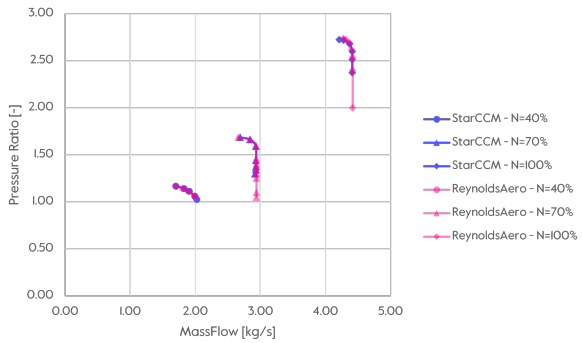


**Fig 11.** ATR engine - Compressor performance map

Indeed, the compressor performance map depicted in Figure 11, that reports the pressure ratio obtained

in the compressor stage as function of the mass flow for three rotational speeds, highlights an excellent agreement between the results obtained with both solvers. In addition, in this map, the results represented for the STAR-CCM+ computations are those performed on the coarse mesh. In fact, a comparison on some points with the fine mesh, showed that the discrepancies were lower than 2%, which led to use the coarse mesh to reduce the computational time for the full compressor map comparison.

#### *4.1.2. Turbine*

Similar analysis and comparison has been performed for the turbine part of the ATR engine. The turbine is made of two stages, with for each stage, a stator followed by a rotor. In this case also the computational domain has been redesigned in Siemens NX CAD software from the reference geometries of the blades, as well as the hub and shroud profiles, in order to generate a polyhedral mesh with similar global parameters as for the compressor described in 4.1.1. However, for the turbine configuration, since each row interface is between a stator and a rotor and vice-versa, the 3.7M hexahedral cells mesh generated by RA is usable in STAR-CCM+ with mixing-plane boundaries at the interfaces. Two polyhedral meshes have been created within STAR-CCM+, a fine one with 5.8M cells, and a coarse one with 0.5M cells.

For this configuration, the simulations were carried out using the one-equation Spalart-Allmaras turbulence model [20]. The model was used by RA for convergence stability purpose, so the same model was selected for STAR-CCM+ computations. The fluid was considered as a mixture of real gases, i.e. hydrogen and water vapour, with a mass fraction of H2 and H2O of 0.475/0.525 respectively, and properties coming from the integrated library.

The results of the computations for one operating point are reported in Figure 12 showing the relative Mach number distribution at 95% of the blade span for two blade-to-blade channels. Figures 12(a) and (c) report the results on the same hexahedral mesh but from different solvers, while Figures 12(b) and (d) report the distribution obtained with STAR-CCM+ solver on two different polyhedral meshed. Overall, the relative Mach number distribution shows a good agreement between the four simulations. Even if the colormap distribution is not exactly the same (due to different post-processing software used) the global trend on high speed and low speed regions is matching quite well between all the computations, even with different mesh types. Like for the compressor part, the coarse grid presents coherent results in comparison to the other finer meshes.

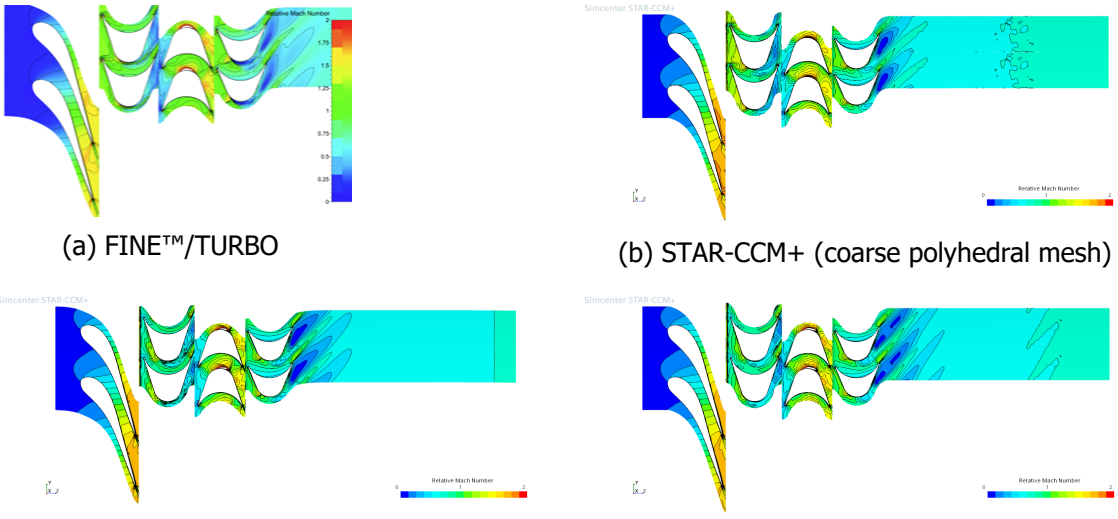

(a) FINE™/TURBO

(b) STAR-CCM+ (coarse polyhedral mesh)

(c) STAR-CCM+ (RA hexahedral mesh)

(d) STAR-CCM+ (fine polyhedral mesh)

**Fig 12.** Relative Mach number distribution at 95% of blade span

The overall performance of the turbine is compared for these four computations. On the different

parameters like the pressure ratio, the isentropic efficiency, the turbine specific work and the turbine power the discrepancies between the four simulations results are under 2%. The turbine performance map is reported in Figure 13, where the isentropic efficiency is drawn as function of the pressure ratio, for three different rotational speeds. Like for the compressor map, for this comparison purpose between the two solvers, the polyhedral coarse grid is used in STAR-CCM+ solver for faster runs at different operating points. Once again the agreement between the results obtained with the two solvers on different meshes is fairly good.

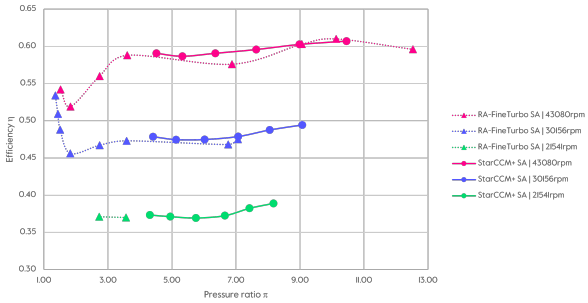


**Fig 13.** ATR engine - Turbine performance map

Finally, the simulations performed with STAR-CCM+ at Destinus on the ATR engine, for the compressor part on one hand, and for the turbine part in the other hand, have shown that the solver is perfectly suited to study and improve the design of these components. The solver STAR-CCM+ provides results similar to those obtained by another CFD solver widely used by turbomachinery manufacturers.

### 4.2. Hydrogen-oxygen pre-burner

In ATR concepts as depicted in Figure 8 , it is possible to rely on other strategies than pumps to drive the turbine. For instance, by making use of a pre-burner. Such possibility has been explored at Destinus with gaseous hydrogen-oxygen. This setup has been a first experience in applying StarCCM+ in a combustion setting. The type of geometry is depicted in Figure 14 showing axial velocity and hydrogen mass fraction contours. Half of the computational domain has been simulated making use of the geometry's symmetrical character yielding a total of $\approx$ 5M cells. In this specific example, fuel and oxidizer are injected coaxially. Supercritical $H_2$ is injected, at a total pressure of 25 bar and total temperature of 300 K, while gaseous oxygen is introduced at the same total conditions. The supercritical character of the fuel introduces the need to consider real gas behavior which is done through the Peng-Robinson equation of state [26]. The 8 species ($H_2$, $O_2$, $H_2O$, OH, H, O, $H_2O_2$, $HO_2$), 21 reactions mechanism of Ó Conaire [27] is considered for $H_2$-$O_2$ combustion. Species individual properties were obtained from the CEA program [28]. Heat capacities are described by the NASA polynomials (7 coefficients) while dynamic viscosities and thermal conductivities were tabulated as a function of temperature. No influence of pressure on the thermodynamic properties were considered which is acceptable given the very limited compressibility as indicated by the compressibility factor ($Z = P/(\rho R T)$) a posteriori. The acentric factors as well as critical pressures and temperatures of each species were specified following the work of Ruiz *et al.* [29]. Mixture properties are obtained through simple mass weighted mixing rules. Unit Lewis number is also considered.

The steady-state solver of StarCCM+ is considered for time stepping. Multigrid cycling has been deactivated (set to 0) in the algebraic multigrid feature as it lead to instabilities in the solution. Inviscid fluxes are treated by a ROE-type FDS solver [30] and turbulence is modeled with Menter's SST approach [21, 31]. Wall functions are enabled to tackle specific regions with a lack of resolution. Turbulent inflow conditions were set to 1 % and 10 for turbulence intensity and viscosity ratio, respectively. The turbulent Prandtl and Schmidt numbers are both set to 0.9. A pressure outlet is specified with a pressure of 19.5 bar. Walls are treated as isothermal at a temperature of 300 K. The grid-sequencing initialization procedure of StarCCM+ is activated which computes a set of inviscid solutions on coarser grids with respect to the original one. Starting from the coarsest grid, each inviscid solution is interpolated on the finer mesh up

till the original mesh size is reached. Four grid levels were selected with a maximum of 100 iterations per level. Ignition is artificially induced through an ignition source in a cylindrical region near the point of injection. The methodology increases, locally, the temperature to evaluate chemical source terms. This is done for a few time steps only.

The simulation predicts a stable lifted flame anchored just downstream the point of injection with temperatures reaching up to 3500 K. The extend of the reaction zone (as indicated by OH mass fractions) is limited to about 1/5th of the combustor length (before the contraction). Near-wall temperatures could reach up to 800 K which indicate a possible need for cooling for this specific equivalence ratio depending on the material of the pre-burner. In general, the solver has shown the capability to handle a real gas combustion situation.

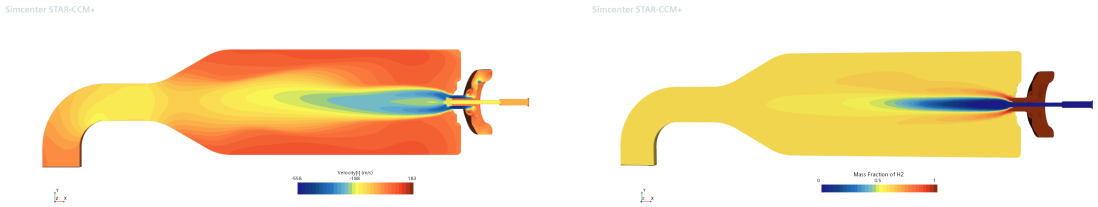

(a) (b)

**Fig 14.** Axial velocity component (x from right to left) (a) and $H_2$ mass fraction (b) in symmetry plane

### 4.3. Pressure losses in injector

An important part of a pre-burner design (see Subsection 4.2) is the injector itself. In order to avoid flashback in the combustion process, a certain level of total pressure drop is required inside the fuel and oxidizer flow paths to act as a buffer. Pressure drops can be achieved through changes in geometrical shape (contractions, bends and expansions) as shown in Figure 15. In order to facilitate the design of injectors, a zero-dimensional Python program has been written relying on the fluids library [32] which contains loss coefficients estimates for standard pipe features including correlations from Idel'chik [33]. Pressure drops can then be estimated from the loss coefficients. Another important point for design is the ability to estimate the mass flow at the exit of the injector as a function of the applied total pressure at the inlet.

CFD has been used to calibrate the zero-dimensional code by comparison of predicted and actual pressure drops as well as evaluating the mass flow rates as a function of applied total pressures. The modeling choices are similar to the ones described in the pre-burner (Subsection 4.2) except that no reactions are considered (only $H_2$ and $O_2$). Moreover, constant thermodynamic properties are applied for each species given the low inlet temperatures. The outlet is modeled as an open surface with same pressure conditions as in previous setup and specified $H_2$ at a temperature of 490 K. By doing so we emulate the density that would be obtained in the case of equilibrium combustion allowing the injected fluids to expand in similar conditions as in a reacting case. Results are presented for type 2 which is simulated with a grid containing 4.3 M cells. The total pressure drop in the fuel side is predicted by the CFD to be 2.89 bar. In the 0D code, only 3 elements were considered to represent the same injector flow path. This discretization can be seen in Figure 16. These elements represent the changes in geometry that would induce the largest total pressure losses which is predicted to be 3.01 bar. The close agreement between both approaches is a very positive result. Given this calibrated piping network for this specific injector geometry, the 0D code is now used to estimate the total pressure required to get a given fuel mass flow rate entering the chamber through a recursive process. Finally, CFD runs are performed with the new fuel inlet conditions to ascertain that the desired mass flow rates are achieved. The result of this exercise is presented in Figure 17 with a very good agreement between predictions and CFD. This is an example where CFD can strongly help in formulating design strategies at a relatively low computational cost.

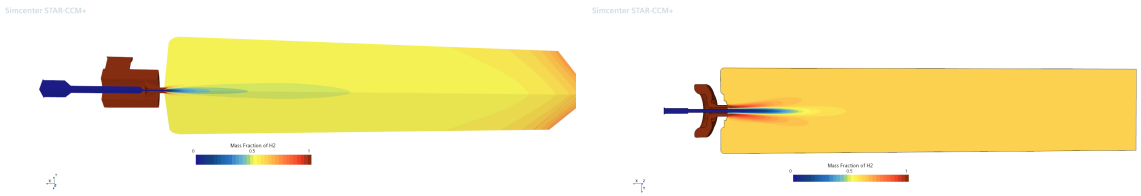

(a) (b)

**Fig 15.** Hydrogen mass fraction contour for two injector heads: type 1 (a) and type 2 (b)

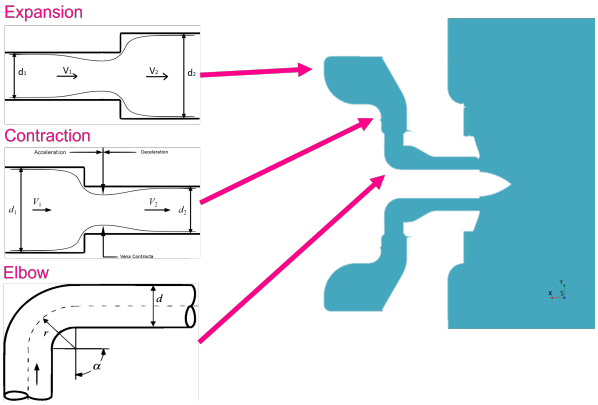


**Fig 16.** Sketch of the injector pointing out the changes in area modelled in the 0D code

## 4.4. Hydrogen-Air mixing

A critical aspect in the overall engine performance is an efficient mixing in the combustion chamber. Careful consideration is especially required in an ATR-like setup (Figure 8) where two flow-paths have to be combined: a fuel path (pre-burned or not) passing through the turbine and an oxidizer path (captured by the intake - compressor flow path). Several activities related to this subject have been undertaken, making use of CFD, and will be briefly detailed below.

### *4.4.1. Generic mixing performance*

One task where CFD can play a key role is to collect performance information with increased level of fidelity. This is best taken advantage of in more generic settings that isolate the physics we're interested in, in this case the mixing behavior. A large range of configurations have been simulated making use of the Java API. The configurations differ in injection hole radius, spacing between injection holes and injection angle as illustrated in Figure 18.

The generic domains are discretized by $\approx$ 600k to 800k cells depending on the setup. The domain was extended in the streamwise flow direction to reduce influence of the exit boundary (modeled as a pressure outlet with back pressure of 2.15 bar) on the mixing behavior. A higher mesh resolution is introduced in the region of interest. Air ($N_2$, $O_2$) is injected at the upper boundary and fuel ($H_2$) is injected at the lower boundary. The inlet mass flows of air and fuel are kept constant throughout the parametric sweep and are specified at total temperatures of respectively 490 and 400 K. Ideal gas behavior is assumed with constant properties for the individual gas components. Turbulence is considered through Menter's SST model ([21]) and inflow turbulence intensities and viscosity ratios are set to 1 % and 10 respectively. Symmetry is used and only half injection holes are simulated. Physical walls in the region of interest are treated adiabatic and slip wall boundary conditions are applied in the downstream region towards the exit plane.

Quantities of interest in the parametric sweep are mixing efficiency (or entrainment), penetration, spread

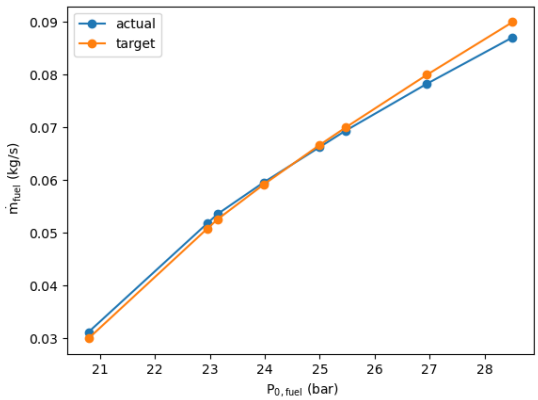


**Fig 17.** Fuel mass flow rates vs. applied total pressure predicted (0D) and actual (CFD) for injector type 2

and total pressure losses as defined in [34]. These are evaluated at several planes from the point of air injection only considering y-coordinates above the injection holes.

The aim of these simulations is to be able to correlate the mixing efficiency to the momentum flux ratio, which is the ratio of velocities and densities of two streams mixing. By this, the optimum ratio of velocities to enhance the mixing in the combustion chamber can be set and the design process of the actual chamber will be simplified to achieve that value.

The importance of the CFD here relies on the difficulty of predicting the behaviour of multiple injection jets and their interaction by numerical methods. Moreover, in the case of the ATR, the fuel cannot be injected in a simple and well-known manner, as the fuel in this combustion chamber comes from the turbine flow. As a result, the mixing mechanism will affect directly to the combustion efficiency, and also to the thrust achieved.

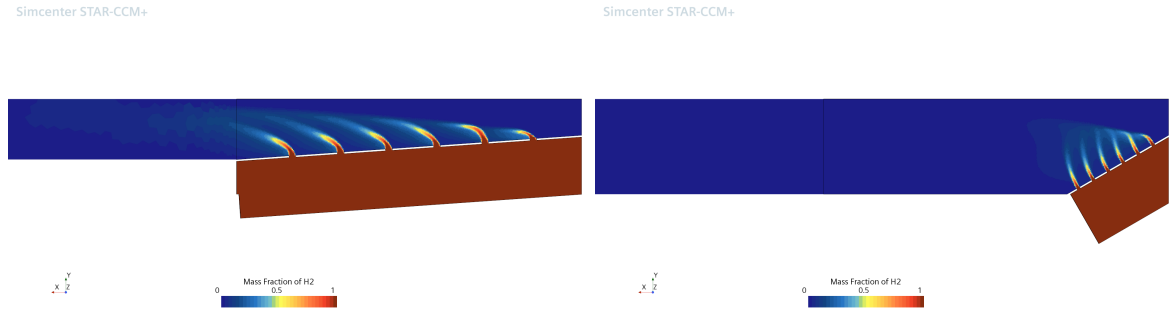


(a) (b)

**Fig 18.** Examples of generic mixing cases with (a) 4 degree inclination, 2 mm hole radius and 2.8 cm distance between holes (b) 30 degree inclination, 1 mm hole radius and 1 cm distance between holes

### *4.4.2. Mixing in combustion chamber*

The mixing behavior was also investigated in actual combustion chambers as illustrated by the different designs in Figure 19. This combustion chamber differs from a regular one in the way fuel and oxidizer are introduced. When talking about an ATR, the combustion chamber is after the turbine, and the fuel comes from the turbine flow. This is why a gas mixer has to be introduced, to mix both streams of fuel (hydrogen or hydrogen and water vapour coming from the turbine) and oxidizer (air coming from the

compressor).

These CFD set ups and the geometries are similar to the cases described in the previous subsection. The aim is also aligned, as the mixing between two streams is analysed. However, in this case, the geometry is bigger, as it is an annular section of 30 degrees of the actual combustion chamber with different gas mixers. As a result, not only the interaction between the jets located in the same vertical row are going to be presented, but also different horizontal rows. Another important aspect is that it has been considered that there is an oxygen pre-burner in this engine, so the flow that comes from the turbine and is introduced to the combustion chamber is a mixture of hydrogen and water vapour. The numerical modeling and spatio-temporal discretization is analogous to 4.4.1. Computational meshes are of the order of 2.3M cells. It was observed that specifying mass flow rates at the inlet, in conjunction with total temperatures, yielded inflow conditions close to the desired ones.

Figure 19 presents the hydrogen mass fraction contours of the same combustion chamber section but with three different gas mixers. Geometrical parameters differ between the cases. The change in parameter is similar to the isolated and simplified mixing cases: the angle of the mixer, and the holes geometry (diameter, spacing and in this case also the number of holes). In this Figure, it can be observed how the change in the gas mixer disposition creates regions of concentration of hydrogen, as well as it changes the air film that protects the walls from the hot combustion products. Due to the complexity of the mixing mechanism, these features cannot be predicted without the use of CFD.

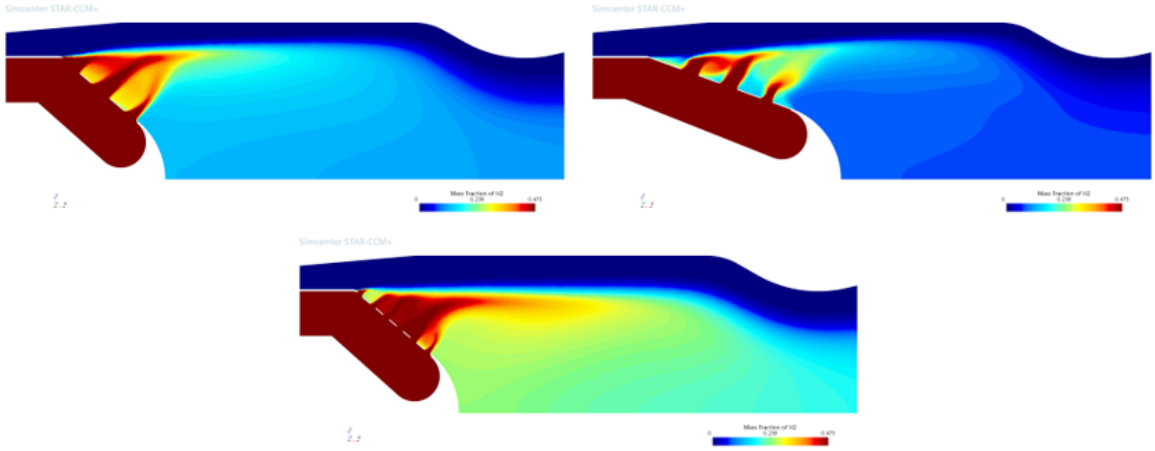

**Fig 19.** Hydrogen mass fraction in mixing simulations inside combustion chamber geometries with different injection mixers

### 4.5. Hydrogen-air combustion

The mixing chamber configurations introduced in 4.4.2 have as well been simulated in a reacting setup. Combustion remains an expensive endeaveour in CFD and is still out of reach for design space exploration in early design purposes. Nevertheless, a number of such simulations can shed light on design problems that cannot be identified otherwise.

The axi-symmetric character of the chamber is used to reduce the computational domain of to a slice. The domain consist of $\approx$ 2.3M cells with some variation depending on the configuration. In terms of numerical setup, the settings are exactly the same as for the pre-burner discussed in Subsection 4.2 except for the fact that a thermally perfect gas is assumed and modeled with an ideal gas law. Simulations with the steady-state solver were started from the converged non-reacting setups and ignition was artificially induced through an ignition source (see also Subsection 4.2). Sensitivity studies to the use of the algebraic multigrid cycling feature have been performed which indicated that it is best to not consider it in such setups. This was also concluded for the pre-burner. It is possible that much finer grids would be required in reacting settings in order to gain advantage from its use. Moreover,

perhaps tuning the different settings of the multigrid cycling could yield better results but has not been explored.

Typical computations required ≈ 762 CPUh to reach a state that can be considered converged with limited mass flow imbalances. One unsteady simulation was considered to evaluate the computational cost to do so. It took close to 7000 CPUh to simulate 1 ms, at which point the simulations were halted given such high demands in computational resources.

Figure 20 shows the mass fraction of OH as well as the temperature in one of the chamber setups. Peak temperatures of 2500 K are predicted. It illustrates the complexity of the mixing process which has to be carefully designed in order to increase mixing (and combustion) efficiencies and create a distributed flame. The flame anchors at the injection plate (not shown here) and introduces very hot localized regions which can lead to material failure. Such information could not be obtained without the use of CFD. A sensitivity on the use of temperature dependent species' viscosities and thermal conductivities has also been performed. It did not shown significant influences on the heat fluxes and temperatures at wall boundaries, and could therefore be omitted in the modeling. This would result in a slight decrease of computational time by avoiding some lookup table steps. This would at least be acceptable for the level of detail that is of interest in relatively early design phases.

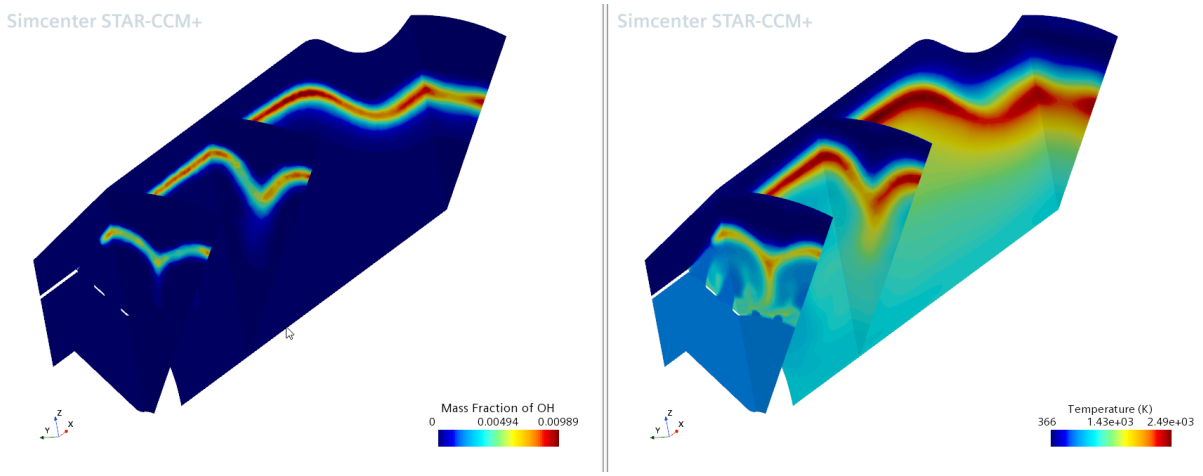


**Fig 20.** OH mass fraction (left) and temperature (right) contour for the reacting chamber case.

### 4.6. Conjugate heat transfer in nozzles

Nozzles are an important part of engine development and require careful considerations with regard to heat treatment. This is especially true for rocket nozzles with combustor exit temperatures in excess of 3500 K associated with heat fluxes of the order of 160 $MW/m^2$ [35]. Understanding and controlling the wall temperatures is essential and can be leveraged in a regenerative cooling setup. CFD can help in this task and requires a conjugate heat transfer setup to model the interaction between the hot fluid in the nozzle and cold cooling liquid through solid walls.

Such setups have been simulated with Simcenter STAR-CCM+ [11] with an example computational mesh shown in Figure 21 where we made use of the axi-symmetrical character of the geometry. The nozzle main fluid is discretized by ≈ 300k cells, the cooling fluid by ≈ 700k cells and the solid by ≈ 250k cells. This cell number ensures that the simulation remains affordable without the need to rely on large computational clusters. Simulations were run on 48 cores for several days.

The nozzle main fluid is modeled as a thermally perfect gas consisting of 8 species ($H_2$, $O_2$, $H_2O$, OH, H, O, $H_2O_2$, $HO_2$). Species individual properties were obtained from the CEA program [28]. Heat capacities are described by the NASA polynomials (7 coefficients) while dynamic viscosities and thermal conductivities were tabulated as a function of temperature. Mixture properties are obtained through simple mass weighted mixing. A unit Schmidt number is assumed to obtain the molecular diffusivity.

Reactions were activated through the mechanism of Ó Conaire [27] for $H_2$-$O_2$ combustion introducing 21 reactions. The cooling fluid is supercritical $H_2$ which is modeled through the Van der Waals real gas equation of state. Temperature dependent properties are specified as a lookup table for heat capacity, dynamic viscosity and thermal conductivity and is generated through the CoolProp Python API [36] which makes use of the NIST database [37]. Solid properties were set to Inconel with constant density and specific heat but temperature dependent thermal conductivity specified through a lookup table. Both fluids' inviscid flux treatments are performed by the AUSM+ FVS [38]. The steady-state solver is selected for time marching. The nozzle main fluid is specified with a total pressure of 4.9 MPa and total temperature of 3500 K. Inlet composition is obtained through the CEA program and yield mass fractions of $H_2$: 1e-4, $H_2O$: 0.0033, OH: 0.9615, $H_2O_2$: 0.0347 and O: 4e-4. The cooling fluid is introduced at a mass flow rate of 0.0125 kg/s (positive y direction) and a total temperature of 40 K. The same mass flow is expected to leave the channel. The solid wall boundaries (left, top and right) are set to adiabatic. The grid-sequencing initialization procedure of STAR-CCM+ is activated which computes a set of inviscid solutions for fluid domains on a sequence of meshes with coarser sizes, interpolating the resulting solution on the finer meshes. It is also important to note that for stability and convergence all three domains needed to be initialized all together.

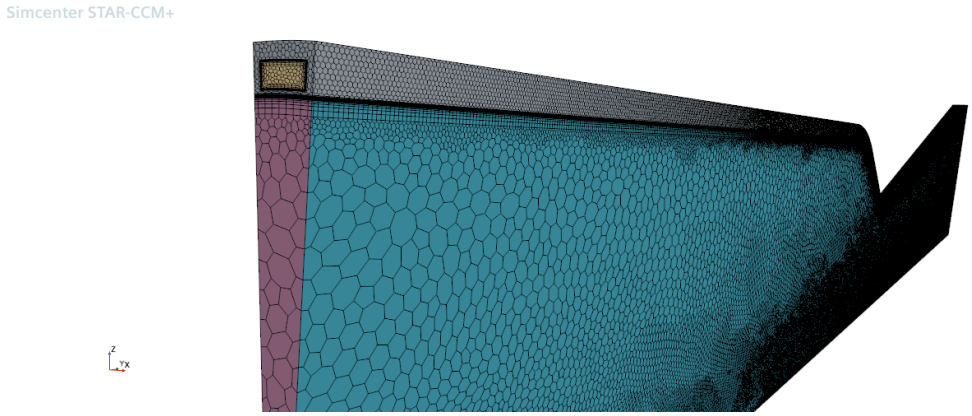


**Fig 21.** Computational mesh of regeneratively cooled nozzle.

The resulting temperature contour is illustrated in Figure 22. It shows the presence of a zone prior to the throat where a considerable amount of heat transfer is occurring. This zone coincides with recirculation of the main nozzle flow and is linked to the change of curvature in the geometry. Such a recirculation is not desirable as it induces localized higher temperatures ($\approx$ 1000 K) which would compromise the integrity of the solid material. Note that the level of chemical reactions is extremely low which indicate that a frozen chemistry assumption could be adopted in such simulations. Overall this exercise has demonstrated that the conjugate heat transfer capability of STAR-CCM+ can be combined with high speed thermally perfect reacting flows and supercritical real gas behavior.

### 4.7. LOx and LH2 pump design

Apart from combustion devices, engine concepts at Destinus require extensive use of turbomachinery. Compressors and turbines are being developed as extensively discussed in 4.1. Furthermore, multiple centrifugal pumps are required to provide the necessary propellants to various combustion devices.

The design of turbomachinery involves a trade-off of many parameters including provisions for strength, cavitation, manufacturability, rotor dynamics and many more. Naturally, such trade-off results in many design iterations which require quick estimate of performance. A one-dimensional Python tool was developed for rapid design exploration. CFD has been used to calibrate the tool against various turbine configurations and ensure reliable predictions.

Traditional design process of centrifugal pumps relies heavily on empirical data. These empirical correlations help in establishing the global parameters of the pump early in the design process. However, they fail

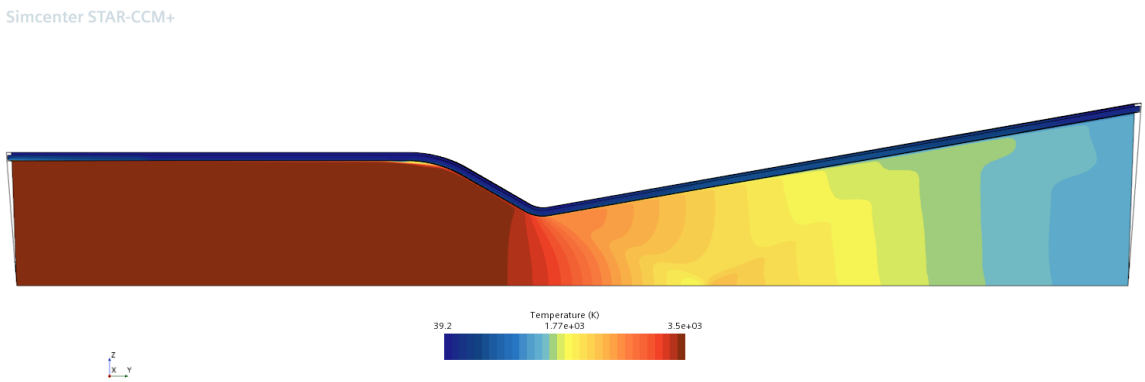


**Fig 22.** Temperature contour of nozzle setup with regenerative cooling.

to capture many of the effects happening in-between the inlet and the outlet. The design process then quickly calls for numerical methods to optimize the design of the flow path.

CFD has been used to evaluate the effect of impeller blade shape on cavitation and performance of the pump. Even though liquid oxygen and liquid hydrogen show a degree of compressibility, the numerical setup was optimized for the speed of iteration. The fluids have been modelled as incompressible with constant thermophysical properties in combination with Spalart-Allmaras turbulence model to facilitate quick design turnover. Following the same philosophy, steady-state solver was selected and interface between each stage was implemented with a mixing plane interface. This approach allowed to model only a single, periodic passage for each blade row. Heat transfer through external walls has been neglected at this stage of design process. A result of one of these simulations is shown in Figure 23. Computational meshes were on the order of 600k cells.

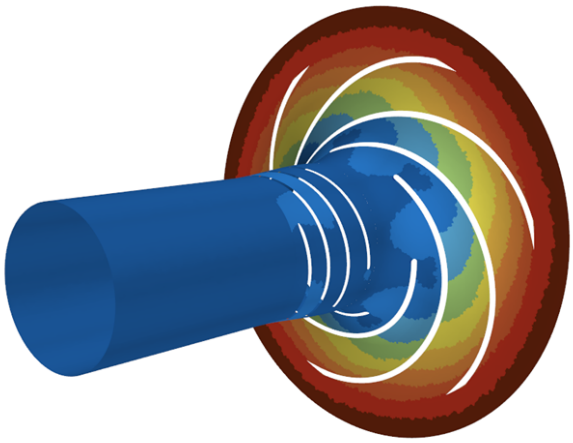

**Fig 23.** Static pressure contour in the design of pump geometries.

## 5. Outlook

The type of problems discussed in Sections 3 did evaluate the solvers' robustness and capability in incompressible, compressible as well as shock dominated external flows, both in inviscid and viscous conditions. In the latter type of problems different meshing strategies have been explored at Destinus including the use of dynamic adaptive-mesh refinement (AMR) as well as static mesh refinement based on user defined criteria extracted on coarser grids. The AMR strategy is well suited for shocks but

can drastically increase cell counts when applied in other regions. In boundary layers for instance, when the aim is to reduce the $y^+$ or increase resolution as to better capture temperature gradients in hypersonic flows, the AMR is not suitable any more due to the isotropic refinement algorithm. Instead, static mesh refinement strategies would be more appropriate. In general, strategies combining AMR (for shocks) and static mesh refinement (other regions of interest) could be devised and is subject to future explorations.

Section 4 lead to the use of chemical solvers for both ideal and real gases. Moreover, a conjugate heat transfer setup has been simulated combining chemical reactions for a thermally perfect gas in supersonic flow and a subsonic supercritical coolant flow modeled as a real gas. Depending on the interest, time stepping has been performed with the steady-state solver or a dual time-stepping strategy. Unsteady time stepping has proven to remain a very computationally intensive task and out of reach for early design purposes. In general, the type of problems did not yet require the need to rely on pressure and temperature dependent thermophysical properties. It is however something that can be expected in the future.

In a less intensive manner, as of yet, the use of CFD has been explored for flow problems in the feed system such as axial pumps and tanks. For the latter problem, stratification was especially of interest. The volume of fluid (VOF) method was therefore applied to describe the multi-phase problem. The intrinsic character of the physical problem requires the use of unsteady time-stepping (dual time-stepping) for long simulation times which becomes already costly for non-detailed design purposes. Moreover, the use of cryogenic hydrogen is extremely challenging from a modeling point of view (phase-change) and is still in active development. Another type of problem, with its own modeling challenges, is cavitation inside pumps. This is specifically challenging in a moving setup such as an axial pump which requires, for instance, the use of overset meshes. Hydrogen related technology is not only a focus at Destinus, but has re-gained interest in Europe for aviation but also other industries. It is therefore to be expected that CFD modeling capability will improve in order to play a key role in related designs.

## 6. Conclusions

The flexibility and capability of the commercial CFD software Simcenter STAR-CCM+ has been extensively challenged at Destinus through application on a variety of problems. The problems are typical ones encountered in hypersonic vehicle design, and its associated components, and differ in complexity from a simulation perspective. The robust meshing capability has proven to be key in ensuring swift generation of computational setups. Together with the API scripting, advanced levels of automation could be achieved which are intensively used in aerodynamic database generation as well as in various parameter sweep studies. The CFD has been useful not only in answering questions but also to identify possible issues. Some limitations, inherent to the complexity of hydrogen-related technologies, have been identified in the solvers with expected improvements on the way.

## Acknowledgements

The authors would like to thank Michael Stubert from Siemens Industry Software GmbH for the continuous support in the use of Simcenter STAR-CCM+. The first author is grateful to Victor Zhukov (Destinus Germany GmbH) for the real gas related discussions and advice in their modeling.

## References

[1] C McClinton. X-43-scramjet power breaks the hypersonic barrier: Dryden lectureship in research for 2006. In *44th AIAA aerospace sciences meeting and exhibit*, page 1, 2006.

[2] J Hank, J Murphy, and R Mutzman. The X-51a scramjet engine flight demonstration program. In *15th AIAA International Space Planes and Hypersonic Systems and Technologies Conference*, page 2540, 2008.

[3] J Steelant, A Mack, K Hannemann, and AD Gardner. Comparison of supersonic combustion tests with shock tunnels, flight and CFD. In *42nd AIAA/ASME/SAE/ASEE Joint Propulsion Conference and Exhibit*, Sacramento, California, July 2006.

[4] KG Bowcutt, A Paull, D Dolvin, and MK Smart. HIFiRE: An international collaboration to advance the science and technology of hypersonic flight. In *Proceedings of the 28th International Congress of the Aeronautical Sciences*, pages 2012–998. ICAS Secretariat RA Leiden, The Netherlands, 2012.

[5] P Roncioni, G Ranuzzi, M Marini, F Battista, and GC Rufolo. CFD aerothermodynamic characterization of the IXV hypersonic vehicle. In *7th European symposium on aerothermodynamics of space vehicles*, pages 9–12, 2011.

[6] S Paris, D Charbonnier, and D Tran. Experimental and numerical investigation of aerothermal characteristics of the IXV hypersonic vehicle. In *7th European Symposium on Aerothermodynamics*, volume 692, page 47, 2011.

[7] SA Berry, ML Mason, F Greene, R King, E Rieken, and K Basore. LaRC aerothermodynamic ground tests in support of BOLT flight experiment. In *AIAA Scitech 2019 Forum*, page 0091, 2019.

[8] BM Wheaton, DC Berridge, TD Wolf, DB Araya, RT Stevens, BE McGrath, BL Kemp, and DW Adamczak. Final design of the boundary layer transition (bolt) flight experiment. *Journal of Spacecraft and Rockets*, 58(1):6–17, 2021.

[9] JP Slotnick, A Khodadoust, J Alonso, D Darmofal, W Gropp, E Lurie, and DJ Mavriplis. CFD vision 2030 study: a path to revolutionary computational aerosciences. Technical report, 2014.

[10] A Cary, , J Chawner, E Duque, W Gropp, B Kleb, R Kolonay, E Nielsen, and B Smith. The CFD vision 2030 roadmap: 2020 status, progress and challenges. Technical report, 2020.

[11] Siemens Digital Industries Software. Simcenter STAR-CCM+, version 2021.3. `https://www.plm.automation.siemens.com/global/en/products/simcenter/STAR-CCM.html`, Siemens 2021.

[12] PG Cross and MR West. Simulation of hypersonic flowfields using STAR-CCM+. Technical report, Naval Air Warfare Center Weapons Division, 2019.

[13] E Schülein, P Krogmann, and E Stanewsky. Documentation of two-dimensional impinging shock/turbulent boundary layer interaction flow. Technical report, 1996.

[14] CG Rodriguez and AD Cutler. Numerical analysis of the SCHOLAR supersonic combustor. 2003.

[15] NJ Georgiadis, DA Yoder, MA Vyas, and WA Engblom. Status of turbulence modeling for hypersonic propulsion flowpaths. *Theoretical and Computational Fluid Dynamics*, 28(3):295–318, 2014.

[16] JMA Longo, K Hannemann, and V Hannemann. The challenge of modeling high speed flows. 2007.

[17] C Cockrell, R Merski, D Witte, and J Mulqueen. Aerosciences, aero-propulsion and flight mechanics technology development for nasa's next generation launch technology program. In *12th AIAA International Space Planes and Hypersonic Systems and Technologies*, page 6948. 2003.

[18] N Viola, P Roncioni, O Gori, and R Fusaro. Aerodynamic characterization of hypersonic transportation systems and its impact on mission analysis. *Energies*, 14(12):3580, 2021.

[19] A Deng. The prediction of aerodynamic performance and handling quality of spaceshiptwo based on the analysis of spaceshipone flight test data. 2012.

[20] P Spalart and S Allmaras. A one-equation turbulence model for aerodynamic flows. In *30th aerospace sciences meeting and exhibit*, page 439, 1992.

[21] FR Menter. Two-equation eddy-viscosity turbulence models for engineering applications. *AIAA Journal*, 32(8):1598–1605, 1994.

[22] G Pezzella, M Marini, B Reimann, and J Steelant. Aerodynamic design analysis of the hexafly-int hypersonic glider. In *20th AIAA International Space Planes and Hypersonic Systems and Technologies Conference, July Glasgow, Scotland*, 2015.

[23] F Roig-Tió, M Suthar, F Miró-Miró, and A Bernabeu-Vazquez. Design of a highly reusable air-turbo-rocket engine. In *73rd International Astronautical Congress (IAC), Paris, France*, 2022.

[24] Cadence Design Systems Inc. OMNIS™/ TURBO & AGILE (INCL FINE™/ TURBO & AGILE). `https://www.numeca.com/product/omnis-turbo-agile`, 2022.

[25] WP Jones and BE Launder. The prediction of laminarization with a two-equation model of turbulence. *International journal of heat and mass transfer*, 15(2):301–314, 1972.

[26] DY Peng and DB Robinson. A new two-constant equation of state. *Industrial & Engineering Chemistry Fundamentals*, 15(1):59–64, 1976.

[27] M Ó Conaire, HJ Curran, JM Simmie, WJ Pitz, and CK Westbrook. A comprehensive modeling study of hydrogen oxidation. *International journal of chemical kinetics*, 36(11):603–622, 2004.

[28] S Gordon and BJ McBride. *Computer program for calculation of complex chemical equilibrium compositions and applications. I.Analysis*. Citeseer, 1996.

[29] A Ruiz, L Selle, B Cuenot, and T Poinsot. Stabilization of a supercritical hydrogen/oxygen flame behind a splitter plate. 2011.

[30] JM Weiss, JP Maruszewski, and WA Smith. Implicit solution of preconditioned navier-stokes equations using algebraic multigrid. *AIAA journal*, 37(1):29–36, 1999.

[31] FR Menter, M Kuntz, and R Langtry. Ten years of industrial experience with the sst turbulence model. *Turbulence, heat and mass transfer*, 4(1), 2003.

[32] C Bell. fluids: Fluid dynamics component of chemical engineering design library (ChEDL), 2016-2021.

[33] IE Idel'chik. *Handbook of Hydraulic Resistance, Coefficients of Local Resistance and of Friction, 1960*. 1966.

[34] WO Landsberg, V Wheatley, and A Veeraragavan. Characteristics of cascaded fuel injectors within an accelerating scramjet combustor. *AIAA Journal*, pages 3692–3700, 2016.

[35] M Pizzarelli, F Nasuti, and M Onofri. Analysis of curved-cooling-channel flow and heat transfer in rocket engines. *Journal of Propulsion and Power*, 27(5):1045–1053, 2011.

[36] IH. Bell, J Wronski, S Quoilin, and V Lemort. Pure and pseudo-pure fluid thermophysical property evaluation and the open-source thermophysical property library coolprop. *Industrial & Engineering Chemistry Research*, 53(6):2498–2508, 2014.

[37] EW Lemmon, IH Bell, ML Huber, and MO McLinden. NIST Standard Reference Database 23: Reference Fluid Thermodynamic and Transport Properties-REFPROP, Version 10.0, National Institute of Standards and Technology, 2018.

[38] MS Liou. Ten years in the making - AUSM-family. *AIAA Paper*, pages 2001–2521, 2001.